SAND2022-0549C

20XX-01-XXXX

Gasoline Direct Injector Deposits: Impacts of Fouling Mechanism on Composition and Performance

Author, co-author (Do NOT enter this information. It will be pulled from participant tab in MyTechZone)
Affiliation (Do NOT enter this information. It will be pulled from participant tab in MyTechZone)

Abstract

Injector performance in gasoline Direct-Injection Spark-Ignition (DISI) engines is a key focus in the automotive industry as the vehicle parc transitions from Port Fuel Injected (PFI) to DISI engine technology. DISI injector deposits, which may impact the fuel delivery process in the engine, sometimes accumulate over longer time periods and greater vehicle mileages than traditional combustion chamber deposits (CCD). These higher mileages and longer timeframes make the evaluation of these deposits in a laboratory setting more challenging due to the extended test durations necessary to achieve representative in-use levels of fouling. The need to generate injector tip deposits for research purposes begs the questions, can an artificial fouling agent to speed deposit accumulation be used, and does this result in deposits similar to those formed naturally by market fuels?

In this study, a collection of DISI injectors with different types of conditioning, ranging from controlled engine-stand tests with market or profould fuels, to vehicle tests run over drive cycles, to uncontrolled field use, were analyzed to understand the characteristics of their injector tip deposits and their functional impacts. The DISI injectors, both naturally and profouled, were holistically evaluated for their spray performance, deposit composition, and deposit morphology relative to one another. The testing and accompanying analysis reveals both similarities and differences among naturally fouled, fouled through long time periods with market fuel, and profouled injectors, fouled artificially through the use of a sulfur dopant. Profouled injectors were chemically distinct from naturally fouled injectors, and found to contain higher levels of sulfur dioxide. Also, profouled injectors exhibited greater volumes of deposits on the face of the injector tip. However, functionally, both naturally-fouled and profouled injectors featured similar impacts on their spray performance relative to clean injectors, with the fouled injector spray plumes remaining narrower, limiting plume-to-plume interactions, and altering the liquid-spray penetration dynamics. , insights from which can guide future research into injector tip deposits.

Introduction

Due to concerns related to carbon emissions from the transportation sector, environmental regulatory agencies continue to implement more stringent fuel consumption (and CO_2 emissions) standards for light duty vehicles (e.g. Euro VI, EPA Tier 3). As a result, automotive Original Equipment Manufacturers (OEMs) have widely adopted strategies to downsize and turbocharge gasoline engine offerings. One key technology enabling this conceptual shift from larger, naturally aspirated engines is direct fuel injection. Benefits of direct injection include reduced knock tendency due to enhanced charge cooling, as well as the potential for improved cold start performance (mainly, reduced unburned hydrocarbon emissions via fast light-off of three-way catalyst) [1,2]. The charge cooling effect resulting from metering fuel directly into the combustion chamber allows for higher engine compression ratios, and improved thermal efficiency. This increase in thermal efficiency is largely responsible for the growth in direct injection adoption in the light duty gasoline vehicle segment (>50% of new vehicle sales for MY2020) [3].

Gasoline direct injection can, however, result in air-fuel mixture heterogeneity due to limited mixing time prior to ignition as well as liquid fuel impingement on combustion chamber surfaces. Both processes lead to increased tailpipe emissions with recent attention focused on particulate matter (PM). Specifically, deficiencies in mixture preparation create fuel-rich zones, and the production of intermediate reaction products that are unable to oxidize sufficiently. In these oxygen-deprived regions, for example, polyaromatic hydrocarbons (PAH) can undergo pyrolysis to produce soot precursors, or PM [4]. Whitaker et al. [5] used Laser Induced Fluorescence (LIF) imaging to provide insight into how fuel impingement (in this case, piston tops) leads to the creation of fuel rich zones and soot formation. Gasoline particulate formation has been shown to be sensitive to fuel composition as well, with a positive correlation between heavier aromatics concentration and increased PM [6,7,8,9].

Deposit formation on injector tips can exacerbate the inherent nature of DISI designs to produce increased particulates as previously mentioned. Injector tip deposits can restrict, and adversely affect spray performance resulting in reduced droplet break-up and atomization; altered spray angle; or changes to spray penetration length [11,12,13]. Either one of these conditions can lead to combustion chamber surface impingement and reduced fuel droplet atomization. In addition to reduced spray performance, tip deposits have been shown to effectively adsorb liquid fuel resulting in late cycle diffusion flame reactions. In work at Delphi, Berndorfer et al. observed presence of a diffusion flame on a coked injector tip following the primary combustion event [10].

The combination of decreasing PM emissions standards (as well as particle number, or PN), implementation of Real Driving Emissions (RDE) in the EU, and the growth of direct injection systems has highlighted the importance of maintaining fuel spray performance in the real world. The literature indicates extensive efforts to better understand injector tip deposit chemical composition with the intent to develop and assess efficacy of deposit control additives (DCA) [14]. The inherent challenges in this type of analysis are 1) the need to consistently, *and* expediently, develop tip deposits; and 2) decoupling the composition of the underlying deposit material versus components that are adsorbed onto the deposit (but may not contribute to growth of the deposit material). Shanahan et al. [155] investigated the use of chemical accelerants to quickly, and reliably, develop injector tip deposits. Specifically, they doped gasoline with DTBDS (di-tert-butyl disulfide) and TBHP (tert-butyl hydrogen peroxide) to mimic effects of sulfur and fuel-aging (respectively) fouling mechanics to achieve statistically significant injector fouling in less than 1500 miles of mileage accumulation (99% CI). Additionally, the presence of sulfur consistently shows up in deposit analyses indicating its critical role in the development of injector deposits.

Gasoline deposit formation mechanisms are believed to occur via both low- and high-temperature reaction pathways [16]. At lower temperatures, oxidation of alkyl radicals can lead to the production of hydroperoxides. As temperatures exceed 350C, high temperature pyrolysis becomes the primary deposit mechanism [11]. Elemental analysis has shown components of both fuel (e.g. C, N, O, S) and lubricants (e.g. Zn and Ph) present in injector deposits [17,18]. Further, researchers have used compositional analysis techniques (e.g. GCMS, FTIR) to provide additional insight into the chemical components present in deposits. Using Fourier transform infrared spectroscopy (FTIR), Von Bacho et al. [179] observed "varnish" deposit composition consisting mainly of hydrocarbons, oxidation, unsaturation, and substituted aromatics. Interestingly, they also inferred through FTIR that deposit composition in various worldwide markets was similar in basic composition indicating less sensitivity to regional differences in fuel qualities and/or contamination.

Based upon the body of research discussed above, the objective of the work described herein is to characterize differences in 1) spray performance (e.g. flow restriction, spray angle, penetration); and 2) chemical composition between injector deposits developed naturally compared to those utilizing profoulant fuels. Further, this work will help guide future fuel injector deposit studies and enable the development of fuel additives optimized for direct injection gasoline engines.

Experimental

Test Engines/Vehicles

This program incorporated injectors sourced from multiple direct injection test vehicles and test engines, represented in Table 1.

Table 1. Summary Table of Test Platform Conditions

Model Year	Make	Model/ Engine	Displacement	Injector Location
2019	Ford	Escape	2.0	Side Mount
2017	Hyundai	Tucson	1.6	Side Mount
2015	BMW	B48	2.0	Central Mount
2014	Honda	Accord	2.4	Side Mount
2016	Honda	Civic	1.5	Side Mount
2012	GM	LHU	2.0	Side Mount

Test Procedures

Ford Escape - A 2019 Model Year (MY) Ford Escape with a 2.0L 4-cyclinder, turbocharged EcoBoost engine with a gasoline direct injection (GDI) fuel delivery system was one of the test vehicles used in this study. Top Tier unleaded fuel was used throughout the entirety of the test and was acquired in large batches to minimize fuel variability during the study. Vehicles were run on a mileage accumulation dynamometer (MAD) using a modified US06 operating cycle to encompass average road and highway driving speeds. The US06 cycle has high acceleration with rapid speed changes. Regular maintenance was conducted as outlined in the owner's manual and the vehicles underwent oil changes on a regularly scheduled interval. Vehicle testing spanned 8 months and was done in an outdoor, covered facility; ambient air temperature, which varied from 18.5°C to 31.5°C (65.3°F-88.8°F), and humidity were not controlled. Long term fuel trim (LTFT), as well as coolant temperature were measured throughout the test with coolant temperatures remaining between 87.0°C -105.7°C (188.6-222.3°F). Fuel injectors (Figure 1) were removed from the vehicle for deposit analysis at approximately 200,000 miles after fuel dilution of the engine oil, as measured by ASTM D3525, remained above 6 mass %. Injector flow restriction was measured by comparing the fouled injectors to new injectors, the injector imaging was completed, and injector tip deposit volumes were measured and also compared to new injectors. The deposited injectors were then utilized for spray analysis and the deposits were subsequently scraped and analyzed via Pyrolysis-Gas Chromatography-Mass Spectrometry (py-GC-MS).

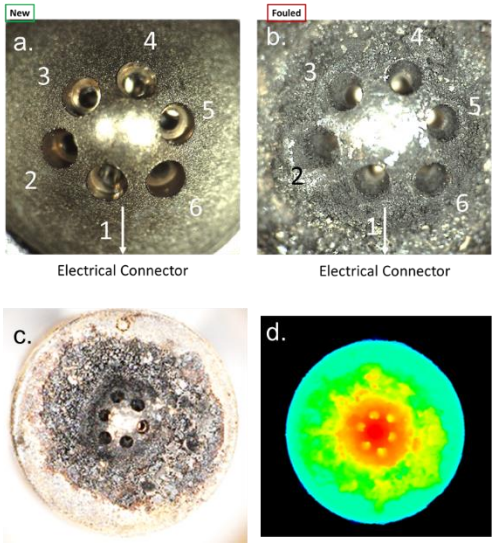

Figure 1. Ford Escape Injector images: a. Close-Up photograph of clean Injector Tip with relative nozzle hole orientation; b. Close-Up photograph of fouled Injector Tip with hole orientation; c. Photograph of fouled injector; d. Height Contour Map of Injector Tip.

Hyundai Tucson – A 2017 1.6L turbocharged Hyundai Tucson was run on a MAD where it accumulated 8,000-miles using a repeating drive cycle. The drive cycle was designed to have repeating segments of low speeds with moderate load and idle [20]. The test conducted for this study was run using a profouled lab-blended fuel designed to maximize the production of injector deposits. Gas Chromatography Detailed Hydrocarbon Analysis (GC-DHA) of the profouled test fuel was performed and it was found to contain 37.6vol% aromatics, including 8.5vol% C10+ aromatics as well as 9.5vol% olefins. The profouled fuel was doped with a sulfur cocktail dopant consisting of a combination of 409ppmw DTBDS and 286ppmw TBHP [15]. This test was run in an outdoor covered facility and humidity was not controlled. Outside ambient temperature during this test showed only modest variation, within 5.6°C (10°F), and coolant temperature was controlled between 78.8°C -93.9°C (174-201°F). At the completion of the mileage accumulation, the injectors (Figure 2) were photographed and injector restriction was measured by comparing the fouled injectors fuel flow volume to the clean, pre-test injector fuel flow volume. The injectors were then utilized for spray analysis and subsequently the deposits on the tips of the injectors were scraped and analyzed via Py-GC-MS.

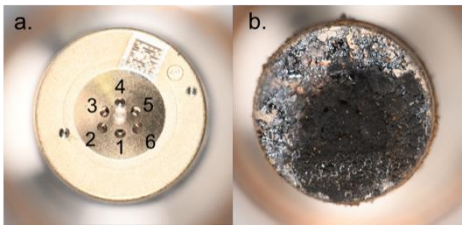

Figure 2. Hyundai Tucson Injector Images: a. Close-Up Photograph of clean Injector Tip and numbered nozzle orientation; b. Fouled injector photograph.

BMW B48 – A 2015 BMW B48 engine with an inline-4 cylinder configuration was used in this test program. This engine stand completed a 96-hour test using a repeating cycle designed to maximize injector deposits, consisting of 5 speed/load stages including idle. This test was run on an additized E10 49-state market fuel and it did not contain a sulfur dopant. Key process temperatures were held steady to limit variability including coolant temperature (100°C), and the inlet air temperature (32°C). At the completion of the mileage accumulation, the injectors (Figure 3) were photographed and injector restriction was measured by comparing the fouled injectors fuel flow volume to the clean, pre-test injector fuel flow volume. The injectors were then utilized for spray analysis.

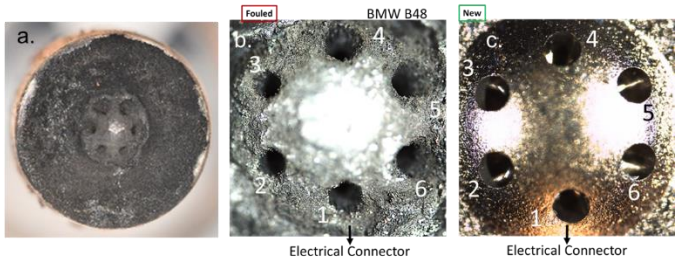

Figure 3. BMW B48 Injector Images: a. Photograph of fouled Injector Tip; b. Close-up photograph of fouled injector tip with hole orientation; c. Close-up photograph of fouled injector tip.

Honda Accord – In contrast to the Escape injector set, which was sourced from a controlled vehicle test, an injector set from a privately registered Honda Accord was analyzed as well. Specifically, this set came from a 2014 model year vehicle equipped with a 2.4L naturally aspirated 4-cylinder direct injection engine. This vehicle accumulated 258,472 miles before the injectors were removed and was fueled predominantly with California compliant gasoline. These injectors were not part of a controlled test; therefore, there is no cycle or temperature data available. Analysis included photo documentation of injector tip condition (Figure 4) and tip deposit collection for Py-GCMS compositional analysis.

Figure 4. Close-Up Photograph of Honda Accord Injector Tip

Honda Civic – Similar to the Accord, an injector set was retrieved from a 2016 Civic model equipped with a 1.5L turbocharged 4-cylinder GDI engine. This vehicle had accumulated 120,837 miles and was fueled predominantly with a 49-state compliant market gasoline. The scope of analysis performed was the same as the Accord described previously (Figure 5).

Figure 5. Close-Up Photograph of Honda Civic Injector Tip

GM LHU – a 2012 2.0L GM LHU engine with an inline 4-cylinder configuration was used in this test program. This engine stand test was run on a profouled fuel consisting of unadditized premium unleaded E10 gasoline doped with a sulfur dopant cocktail made from a combination of 409ppmw DTBDS and 286ppmw TBHP [15]. GC-DHA was performed on this fuel blend and it was found to contain 29.7vol% aromatics, including 3.9vol% C10+ aromatics as well as 7.0vol% olefins. In order to maximize the production of injector tip deposits over the span of this 100-hour test, a low speed/low load (1450RPM/60Nm) steady-state test cycle was chosen. All other operating conditions were held steady to limit variability including coolant temperature (96°C), the oil sump temperature (96°C) and the inlet air temperature (32°C). At the completion of the test, the injectors (Figure 6) were photographed and injector restriction was measured by comparing the fouled injectors fuel flow volume to the clean, pre-test injector fuel flow volume. The injector tip deposit volumes were measured and also compared to clean, pre-test injectors. The deposited injectors were subsequently scraped and analyzed via Pyrolysis-Gas Chromatography-Mass Spectrometry (py-GC-MS).

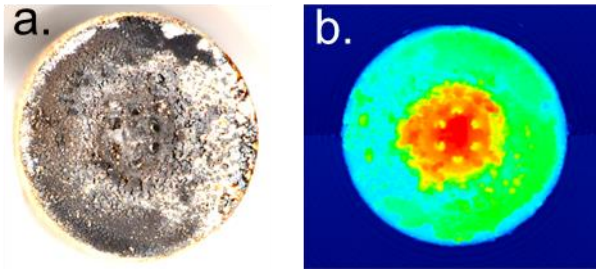

Figure 6. GM LHU Injector images: a. Close-Up photograph of Injector Tip; b. Height Contour Map of Injector

A Summary of the test conditions and analysis performed can be found in Table 2 and Table 3

Table 2. Summary Table of Test Platform Conditions

Test Platform	Test Length	Test Cycle	E10 Additized Market Fuel	Profouled Fuel
Ford Escape	200K-mi	Modified USO6	x	
Hyundai Tucson	8K-mi	Low Speed/ Moderate Load		x
BMW B48	96-hr	5-stage cycle	x	
Honda Accord	258K-mi	Road	x	
Honda Civic	121K-mi	Road	x	
GM LHU	100-hr	Steady State 1450rpm /60Nm		x

Table 3. Summary of Analysis

Test Platform	Analysis Type				
	GC-DHA	Py-GC/MS	Injector Spray Analysis	Injector Flow Data	Tip Deposit Volume
Ford Escape		x	x	x	x
Hyundai Tucson	x	x	x	x	
BMW B48			x	x	
Honda Accord		x			
Honda Civic		x			
GM LHU	x	x		x	x

Macroscope Scan Procedure

A Keyence VR-3200 was used to measure the deposit volume located on the tip of the gasoline direct injectors used in this study. The VR-3200 measures the volume of physical objects placed in a user-defined volume. In order to determine the volume of injector tip deposits, a subtraction method was used to subtract the volume of a clean injector from the volume of a deposited injector. To ensure repeatability of the measurement, an injector holder was utilized that allowed the injectors to be repeatably located in the same position through multiple scans (Figure 7). The area for measurement is set as surface area for each individual injector type and can be controlled

manually. Magnification of the VR-3200 is set to 50x magnification. This apparatus was used in its standard mode, with brightness and stitching set to auto. The fouled injectors were scanned and a volumetric data point was generated in mm3, after which a new injector was also scanned and an additional volumetric data point was generated. The total volume of the injector tip deposits is calculated as the difference in measured volume between the fouled injectors and the new injector.

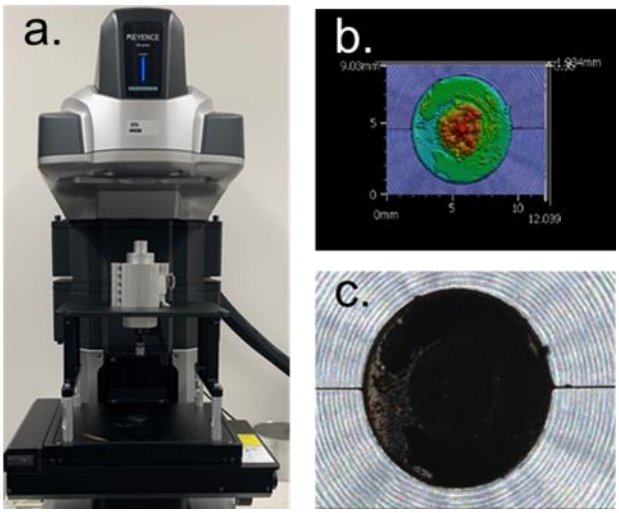

Figure 7. a. Keyence VR-3200 Macroscope with Injector Holder; b. Sample computed deposit thickness; c. Sample injector raw-image.

Injector Spray Analysis

Constant flow vessel for spray optical diagnostics

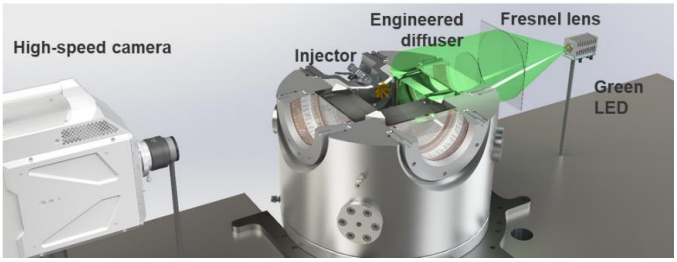

Figure 8: Constant flow spray vessel cross-section and visualization set-up

Optical spray experiments were performed in a constant-pressure, constant-flow vessel at the Combustion Research Facility, Sandia National Laboratories as shown in Fig. 8. High-speed extinction imaging was performed through two optical windows made of quartz. Temperature-controlled injectors are mounted in a side port and fuel sprays are delivered into a temperature and pressure controlled ambient environment. Nitrogen gas flows slowly (at approximately 0.1 m/s) through the vessel to scavenge fuel between injections to permit acquisition of large, statistically converged datasets. The nitrogen flow enters a heating coil surrounded by an insulator piece at the bottom part of the vessel and then moves through a diffuser to enhance uniformity in the velocity and temperature field. The mixture is then replaced by a fresh charge of ambient gas before the next injection. For some conditions, a customized vacuum pump is used to reach sub-atmospheric conditions in the vessel. Further details of the spray vessel and optical setup can be found in [21,22,23]

Liquid spray imaging

The liquid spray was identified by diffused backlit extinction imaging with two different setups. The engineered diffuser supplied a homogeneous light field and suppressed beam steering by evaporation or temperature field in the vessel. This imaging technique is designed to collect extinction only by the fuel in its liquid phase, and not from its vapor. In the first setup, a high-speed green light-emitting diode (LED), Fresnel lens (150mm, f=150mm), engineered diffuser (20°), and band-pass filter (center wavelength: 527nm, bandwidth: 20nm, full width-half max: 22nm) were utilized. A high-speed digital video camera (Photron, SA-Z) equipped with a prime lens (Nikkon, 50mm f/5) was used to capture images of the spray development in the vessel. The green LED was operated with a 24ns command signal (~220ns LED flash time) duration to freeze the spray in the visualized frame. The imaging was performed at a shutter speed of 67,200 frames per second (fps) with an image resolution of 512 by 512 pixels. The aperture of the lens and exposure time of the high-speed camera was set to 2.8 and 13.27µs, respectively. In the second setup, a long-distance microscopic lens (Infinity, K2) was utilized for extinction imaging of near-field plume dynamics. The images were taken at 20,000 frames per second (fps) with a pixel resolution of 3.8 µm / pixel.

The injector is installed in the chamber with a rotating stage that enables the precise angle alignment with the secured sealing of chamber and fuel pressure. This allows the viewing angle of the spray to be varied with a fixed camera to obtain the extinction images at the different viewing angles needed for 3D computed tomography (CT) reconstruction. Imaging was performed at 72 different viewing angles (injector rotating angle) from 0° to 177.5° with 2.5 degrees intervals while 25 injections were recorded for each injector position.

Image processing method

Projected liquid volume (PLV) measurement - Extinction imaging is recommended by the Engine Combustion Network community for spray characterization because it can provide more quantitative information for liquid fuel concentration than conventional Mie-scattering imaging associated with lighting and scattering uncertainties [24]. Using the measured optical thickness, droplet size, and extinction coefficient, the projected liquid volume (PLV) along a line of sight can be derived for direct comparison with CFD results. The optical thickness in a spray region can be calculated based on the Beer-Lambert law as follows:

$$\tau = -\ln(I/I_o)$$

Equation 1. Beer-Lambert Law

where I is transmitted attenuated light intensity due to interaction with the liquid spray, and I_o is incident light intensity without any extinction. This level of transmission intensity is reasonable for detection of the spray outline above the noise floor of the camera, but the vapor-phase beam steering needs to be considered and accounted for using engineered diffusers. The measured optical thickness τ is correlated to the PLV, which is the integral of liquid volume fraction (LVF) along the cross-stream direction y, as follows:

$$PLV = \tau \frac{\pi d^3/6}{C_{ext}} = \int_{-y_\infty}^{y_\infty} (LVF) \cdot dy$$

Equation 2. Projected liquid volume calculation in cross-stream direction y

Mie-scattering and extinction theories were applied in Equation 2, along with assumptions that droplet diameter d and extinction coefficient C_{ext} do not vary along the line of sight. The PLV indicates how much liquid volume is in a certain projected area, so it has a unit of mm^3(liquid)/mm^2. To derive PLV quantitatively, the important parameters, such as d and C_{ext}, should be quantified. In particular, C_{ext} is a function of a droplet size, wavelength of light, and collection angle of the receiving optics, with calculated values available using MiePlot [22]. In this study, droplet diameter was assumed to be 7 μm [23], based upon direct measurement in GDI sprays, which yields $C_{ext} = 72.7 \cdot 10^{-6}$ mm^2 for the optical setup of the study.

3D computed tomography - At each injector rotation view, an ensemble average of 25 injections was normalized by a background image absent of spray to perform the calculation of PLV using Equation 2. Mixtures very near the injector may be too optically thick for reliable measurement of PLV, but analysis in dilute regions downstream of approximately 15 mm of the injector provide suitable information for liquid plume dynamics.

PLV data for the spray rotated to 72 different viewing angles were transformed into 3D spray by a CT algorithm. Since the PLV data are available at 72 viewing angles from 0° to 177.5°, the 'full view' CT reconstruction could be conducted. The reconstruction was carried out by using a built-in 'iradon' function in MATLAB which uses the filtered back-projection algorithm to perform the inverse Radon transform.

Test conditions

Table 4. Spray Experimental Conditions

ECN Condition	G2			G3			2 bar	
Description	Flash boiling			Early injection			Boosted	
Injector	B48	Tucson	Escape	B48	Tucson	Escape	Tucson	Escape
Injected Mass Qinj [mg]	-	20	-	-	20	-	20	-
t inj dur [ms]	0.8	1.63	0.92	0.8	1.63	1.84	1.63	3.68
Injection Pressure Pi [bar]	200	100	100	200	100	100	100	100
Fuel Temperature Tfuel [K]	363	363	303	363	363	303	363	303
Ambient Pressure Pa [bar]	0.5			1			2	
Ambient Temperature Ta [K]	333							
Ambient Density ρa [kg/m3]	0.5			1.01			2.02	
Fuel	RD5-87							

The spray experiments were carried out under charge-gas conditions based upon ECN Spray G's [25] G2 and G3 conditions, which correspond to early injection under low engine load condition and early injection under high engine load conditions. The ambient pressures were 0.5 bar and 1 bar for G2 and G3 respectively. An additional condition based on G3 but with an ambient pressure of 2 bar was used for the Hyundai Tucson and Ford Escape injectors to simulate boosted conditions. The ambient temperature was set to 333 K for all conditions. The temperature of the injector tip was maintained by a water circulator at 363 K during the experiments. The injection quantity was set to 20 mg for the Hyundai Tucson injector and 10 mg for the BMW B48 injector. The injection quantity for the Ford Escape injector was varied with the condition by changing the injection duration to 0.92, 1.84, and 3.68 ms for the respective cases. For the Ford Escape injector, all results discussed in this work are sampled before end of injection and invariant on the ultimate injected quantity. The RD5-87 fuel is a reference E10 gasoline meeting U.S. EPA Tier 3 certification specifications with extensive details of the fuel provided in Ref [26]. The details of the experimental conditions are summarized in Table 4.

Pyrolysis Gas Chromatography/Mass Spectrometry

Pyrolysis Gas Chromatography/Mass Spectrometry (Py-GC/MS) analyses were carried out using a Frontier auto-shot sampler (AS-1020E) with a multi-shot pyrolyzer (EGA/Py-3030D) and a selective sampler (SS-1010E) utilizing a micro jet cryo trap (MJT-1030Ex) on an Agilent 7890A gas chromatograph coupled to an Agilent 5975C mass spectrometer with an electron ionization source.

Approximately 0.1 mg of injector tip deposit was introduced into the pyrolyzer. A multi shot experiment was used to perform GC/MS analysis on thermal desorption and pyrolysis vapor products. First, the sample was ramped from at 100-200 °C and held at the final temperature for 3 minutes. Volatile components were evolved and directed with a split ratio of 25:1 into the cryogenic trap inside the GC oven. The remaining sample was then removed from the pyrolysis inlet by the selective sampler to allow for GC/MS analysis of the evolved gases from the initial temperature regime. The sample was then reintroduced to the pyrolyzer after GC/MS analysis was completed for the gases that evolved from 100-200 °C and the

process was repeated in the temperature ranges of 200-300 °C, 300-400 °C, and 400-1050 °C yielding a total of four GC/MS chromatograms for each injector tip deposit sample.

For GC/MS analysis of the evolved gases, the cryogenic trap was released and the GC oven containing a UA-5 column (5% phenyl/95% poly dimethyl siloxane) 30 m x 0.25 mm (0.25 µm film) was held at 40 °C for 2 minutes, then ramped to 180 °C at 2.5 °C/min, then ramped to 300 °C at 20 °C/min, then held at 300 °C for 3.5 min. The GC inlet temperature was 300 °C, the mass spectrometer transfer line temperature was 320 °C, the EI source temperature was 230 °C, and the quadrupole temperature was 150 °C.

Results & Discussion

Injector Restriction

Injectors from the Ford Escape, GM LHU, BMW B48, and Hyundai Tucson test platforms were collected and subsequently tested in an injector flow apparatus, measuring the volume of fluid being pumped out of the injector at the 1.5ms pulse width. The total volume of fluid from fouled injectors were then compared to the volume of fluid from new injectors to give a percent injector restriction value. These values for each individual injector as well as the average injector restriction from the different test platforms can be found in Table 5.

Table 5. Measured Injector Flow Restriction at 1.5 ms pulse width.

Test Platform	Individual % Injector Restriction				Average % Restriction
	Inj 1	Inj 2	Inj 3	Inj 4	
2019 Ford Escape	13.6	13.0	14.5	10.4	12.9
2012 GM LHU	10.7	16.9	13.2	13.6	13.6
2015 BMW B48	1.2	0.7	1.3	1.4	1.1
2017 Hyundai Tucson	9.0	8.1	13.9	11.9	10.7

This data demonstrates how different fueling and testing strategies can affect to what extent injectors can be restricted. In the case of the GM LHU injectors as well as the Hyundai Tucson injectors, injector restriction was achieved in a relatively short test duration, using a sulfur dopant (profoulant) in the fuel. In the case of the Ford Escape, the restriction was achieved through long-term testing (200,000-miles) over the span of 8 months with an additized market fuel. The BMW B48 injectors had only very minor levels of restriction because of the short time duration for the test, 96 hours, and the use of an additized market fuel.

Injector Volume Measurements vs. Injector Fouling Measurements

Injector tip deposit volumes were measured using the Keyence VR-3200 apparatus and they were compared to flow restriction measurements to understand how the tip deposit and flow restriction is affected by different fuel and cycle conditions. The results are presented in Figure 9, where the injector flow restrictions and the injector tip deposit volumes are plotted for both the Ford Escape injectors as well as the GM LHU injectors. These two test platforms are:

1. Ford Escape - a platform where the injectors were restricted naturally through high mileage, approximately 200k miles, using an additized market fuel

2. GM LHU - a test platform where the injectors were fouled through the use of a chemical sulfur dopant over the course of a 100-hour test.

In the case of both test platforms, there is no correlation between injector tip volume and injector flow restriction. What can be observed in this data is that the volume of deposits present on the tip of the injector using a profouled fuel, from the GM LHU engine, is higher than the volume of deposits on the tip of an injector that used a market fuel over a higher mileage, the Ford Escape vehicle, even though the injectors were restricted to a similar extent. This indicates that the profouled fuels could have a tendency to produce a higher volume of deposits, than what might naturally be formed over time in a vehicle on the road. This artificial deposit growth could have a negative effect on the injector spray morphology.

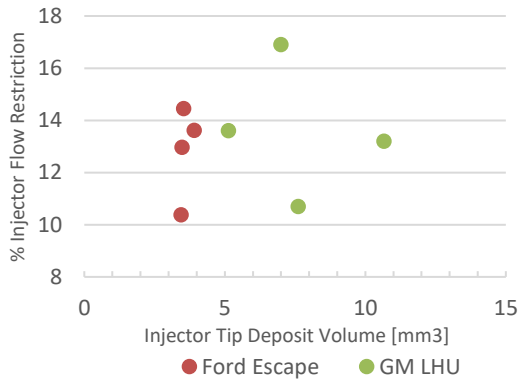

Figure 9. Injector Flow Restriction versus Injector Tip Deposit Volume of GM LHU and Ford Escape injectors

Pyrolysis Gas Chromatography/Mass Spectrometry

Chemical analysis of injector tip deposits is an important tool in trying to elucidate the difference between tip deposits formed through the use of a profoulant and deposits that are formed naturally over longer drive intervals with additized market fuel. In this section we focused on five different test platforms to help us study this point, where two of the test platforms utilized a profouled fuel and three of the test platforms utilized market fuel:

1. 2017 Hyundai Tucson – 8,000-mile test with a profouled fuel
2. 2014 Honda Accord – 260,000-mile interval with market fuels
3. 2016 Honda Civic – 120,000-mile interval with market fuels
4. 2012 GM LHU – a 100-hour test with a profouled fuel

5. 2019 Ford Escape – 200,000-mile test with a market fuel

In general, the pyrolysis gas chromatography/mass spectrometry (Py-GC/MS) reconstructed total ion current chromatograms (RTICC) contain three distinct regions. Very low molecular weight gases are detected in the first region, which is from 2-5 minutes on the RTICC. The first peak detected in this region is carbon dioxide (CO_2) which could be an artifact of the cryogenic trapping. The second region is from 5-12 minutes, where mononuclear aromatic compounds, including some containing oxygen and nitrogen (mainly for the pyrolytic temperature regimes), are detected. The third region is from 12-30 minutes, where dinuclear and polynuclear aromatic compounds are detected. None of the RTICC contain significant peaks after 30 minutes. The RTICC for the 100-200 °C Py-GC/MS temperature regime of the profouled injector tip deposit from the GM LHU is shown in Figure 10 along with the demarcations for the different regions of the chromatogram.

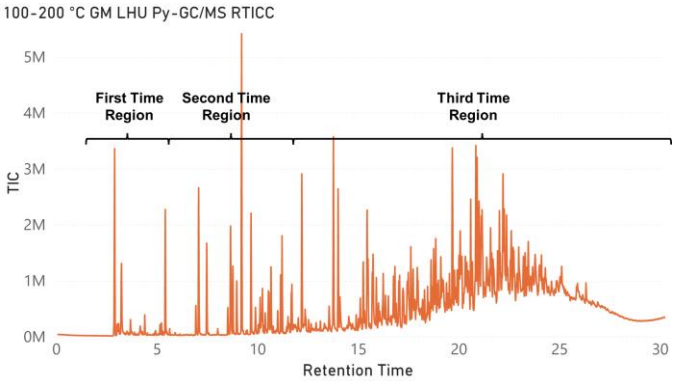

Figure 10. RTICC of the 100-200 °C Py-GC/MS temperature regime of the profouled injector tip deposit from GM LHU.

It is reasonable to assume that in the 100-200 °C temperature regime of the Py-GC/MS experiments that there will only be thermal desorption of volatile and semi-volatile molecules from the deposits. The gases that evolve from the deposits are likely related to the composition of the fuel and the adsorption characteristics of the deposits. It is difficult to derive meaning from the relative intensities of the RTICC peaks when comparing the deposits with each other. Differences in handling and ambient exposure conditions could affect the quantity of volatile and semi-volatile molecules still adsorbed in the deposit at the time of analysis. Additionally, there may be slight variations in retention times of peaks due to the cryogenic trapping of volatile gases. There tends to be greater consistency as the compounds get heavier.

A qualitative comparison across all of the RTICC in the 100-200 °C temperature regime (Figure 11) shows the gases evolved from the deposits to be very similar in the first two regions of the chromatograms. The vast majority of molecules that are detected are hydrocarbons. All of the deposits evolve light hydrocarbons in the early time region (Supplemental Figure S.1), such as pentane and 2-methylbutane. With the exception of the deposit from the Hyundai Tucson, all of the deposits evolve ethanol here as well. This is consistent with the fact that the fuel used in the Hyundai Tucson was an E0 whereas all other fuels contained ethanol.

The peak distribution for the second time region from 5-12 min (Supplemental Figure S.2) are nearly identical. Since these molecules are likely from gasoline that has adsorbed into the deposit, it is similar to looking at the peak distribution of a gasoline's GC-DHA chromatogram. In GC-DHA analysis, most gasoline samples are shown to contain the same molecules, but different relative abundances.

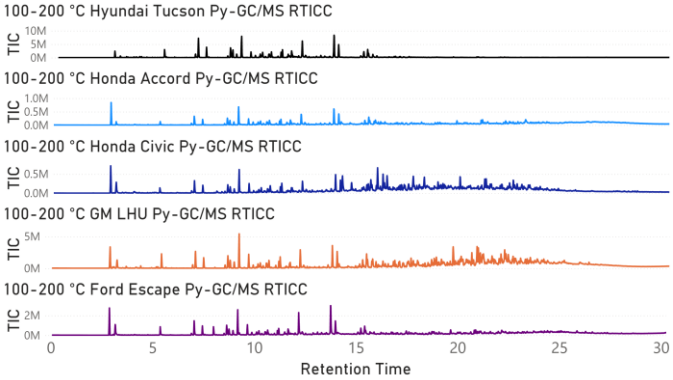

Figure 11. Comparison of the RTICCs from all injector tip deposits in the 100-200 °C Py-GC/MS temperature regime

As can be seen from the comparison of the RTICC in Figure 11 the major difference is in the third time region (Supplemental Figure S.3). Most of the compounds detected here are polynuclear aromatics. The relative amount of these compounds varies from there being no significant polynuclear aromatics in the Hyundai Tucson injector tip deposit to a high relative amount of polynuclear aromatics in the Honda Civic and GM LHU injector tip deposits. It is possible that these differences are related to the fuel compositions used to generate the deposits, the adsorption/desorption characteristics of the deposits, or a combination of both factors. The absence of polynuclear aromatics in the Hyundai Tucson is notable when considering that the fuel is known to have contained heavy aromatic compounds (8.5vol% C10+ aromatics). The only unique difference is that the fuel was an E0 and all of the other fuels contained ethanol. It is possible that the absence of ethanol affected the affinity of the deposit for polynuclear aromatic compounds. This could be due to ethanol's high heat of vaporization which in turn leads to the other fuel molecules experiencing lower temperatures making it more difficult for them to evaporate[28].

It is likely that a majority of the volatile and semi-volatile molecules adsorbed to the deposit would have desorbed in the 100-200 °C Py-GC/MS temperature regime unless there are effects that cause stronger adsorption, such as hydrogen bonding or acid/base interactions. The 200-300 °C Py-GC/MS temperature regime is too low in thermal energy for pyrolysis of carbon-carbon bonds with typical bond energies, so gases that evolve from the deposits are either volatile or semi-volatile molecules that adsorb more strongly to the deposits or are due to the decomposition of thermally labile bonds. The expectation is that there will not be many gases evolved from the deposit for this portion of the Py-GC/MS experiment.

A qualitative comparison across all of the RTICC in the 200-300 °C temperature regime (Figure 12) shows that significantly fewer peaks are detected from gases evolving out of the deposits in this temperature range. However, for the two injector deposits that were formed using profoulant spiked fuel, key features are observed. First are broad peaks from 3.5-4 min in the first time region (Supplemental Figure S.4) that have mass spectra consistent with sulfur dioxide. Sulfur dioxide is not likely adsorbed as a gas in the deposits and therefore must be a decomposition product of thermally labile

oxidized sulfur compounds in the deposit. These compounds are likely formed as a result of the oxidation of the profoulant sulfur molecules that were added to the fuel. These peaks are entirely absent in the deposits formed from market fuels in this temperature regime. Additionally, there are mononuclear and dinuclear aromatic compounds evolved from the Hyundai Tucson deposit and mononuclear, dinuclear, and polynuclear aromatic compounds evolved from the GM LHU deposit. It is notable that once again polynuclear aromatics are not detected evolving from the Hyundai Tucson deposit.

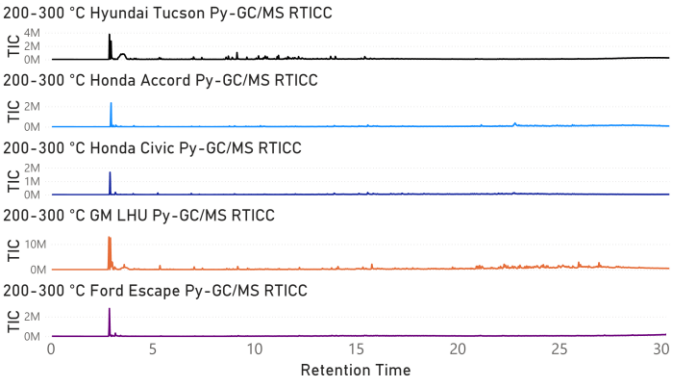

Figure 12. Comparison of the RTICCs from all injector tip deposits in the 200-300 °C Py-GC/MS temperature regime

An initial look at the qualitative comparison for the RTICC in the 300-400 °C temperature regime (Figure 13) shows similarities for all of the samples. In addition to the typical aromatic compounds that have been detected in the previous temperature regimes, heteroatom containing aromatic compounds are detected at this higher temperature range. Specifically, aniline, phenol, and some of their alkyl homologs are evolved from all of the deposits. A qualitative comparison of the extracted ion chromatograms for these compounds shows peaks consistent with C_0-C_3 alkyl aniline and C_0-C_3 alkyl phenol compounds (Figure S.5). It is possible that these compounds are either chemically bound to the deposit and their bonds are thermally labile, allowing them to break at relatively low temperatures, or they are adsorbed strongly to the deposit through hydrogen bonding or acid/base interactions and require higher temperatures to desorb than the compounds detected in the two lower temperature regimes. Additionally, sulfur dioxide peaks are present in the RTICC for the deposits that were formed in the profoulant spiked fuels but are absent in the deposits that formed from market fuels in this temperature regime.

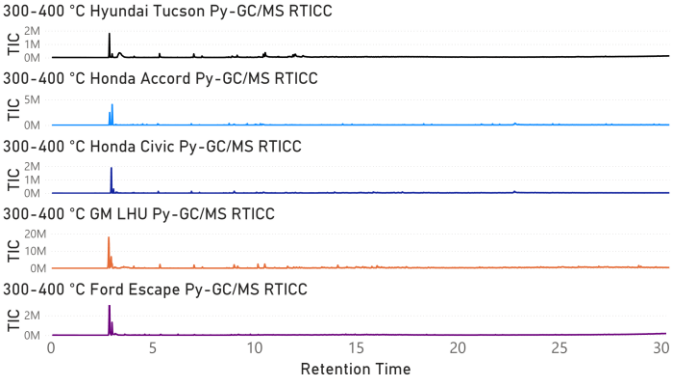

Figure 13. Comparison of the RTICCs from all injector tip deposits in the 300-400 °C Py-GC/MS temperature regime

The final temperature regime for the Py-GC/MS analysis of the injector tip deposits is 400-1050 °C. These temperatures are high enough to cause the pyrolysis of many chemical bonds [27]. Analysis of deposits by pyrolysis is a complex process and it is difficult to know the amount of the injector tip deposit that is ultimately pyrolyzed and evolved as gaseous molecules and the amount that remains in the oven as coke. A comparison of the RTICC for the five deposits in this temperature regime (Figure 14) shows that a number of the most abundant peaks are the same across all of the deposits. These peaks are consistent with mononuclear aromatic compounds including benzene, toluene, and C_8 aromatics. The RTICC from injector tip deposits that came from fuel spiked with profoulant still have peaks consistent with sulfur dioxide evolving from the deposit. However, in this temperature regime evidence for sulfur dioxide evolution is observed for the other deposits as well. This can be seen by creating an extracted ion chromatogram for *m/z* 64 (Supplemental Figure S.6). The sulfur dioxide peaks are relatively small in the deposits from fuels that do not contain profoulant. This could be indicative of naturally occurring sulfur molecules oxidizing and becoming incorporated into the deposit. Alkyl phenol and alkyl aniline compounds are found in all of the RTICC for the final temperature regime as well. This suggests that these molecules are incorporated into the deposit and not just adsorbed to it. The deposit from the Ford Escape has a peak at 6.3 minutes that is consistent with a hexamethylcyclotrisiloxane which is typically attributed to column degradation. This could be an artifact of the analysis although this is not likely since it is only observed in this single sample. Also, repeated analysis of these deposits shows the result is reproducible. It could be a contaminant from the deposit scraping process. It could also be part of the deposit possibly coming from other sources such as the lubricating oil used in the engine.

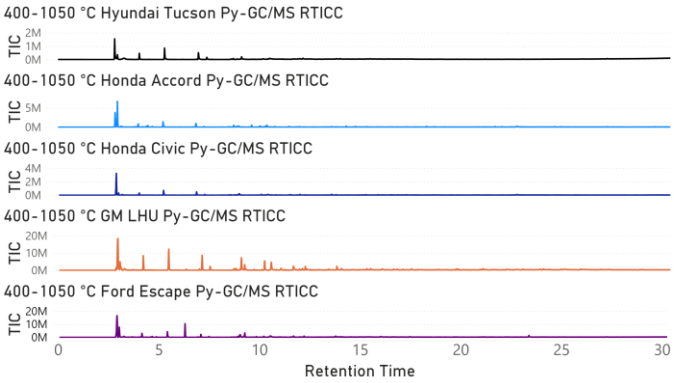

Figure 14. Comparison of the RTICCs from all injector tip deposits in the 400-1050 °C Py-GC/MS temperature regime

Injector Tip Deposit Analysis

When comparing the compounds that are detected in the Py-GC/MS experiments for the different deposits some key observations have been made. The adsorption/desorption characteristics are slightly different between the deposits, which is seemingly related to the ethanol content of the fuel used. This appears to affect the polynuclear aromatic content adsorbed to the deposit. The E0 fuel does not evolve polynuclear aromatics whereas all of the other deposits which were formed with E10 do evolve polynuclear aromatics to some degree. It is unlikely that the polynuclear aromatic compounds are native to any of the gasoline samples so the presence of ethanol may also be affecting the formation of the polynuclear aromatic compounds and not just their ability to adsorb to the

deposits. Overall, aromatic compounds are observed throughout all of the temperature regimes in all of the deposits and are likely the core structural moiety of the injector tip deposits.

All of the deposits evolve sulfur dioxide in the 400-1050 °C temperature regime in the Py-GC/MS experiments. However, the deposits that were formed using profoulant begin to evolve sulfur dioxide in the 200-300 °C temperature regime and continue throughout. It is unlikely that sulfur dioxide gas is adsorbed into the deposit so it must be evolving from thermally labile oxidized sulfur compounds in the profouled deposits. These compounds are likely forming from the oxidation of the sulfur molecules in the profoulant sulfur cocktail during engine operation, incorporating into the injector tip deposit either through adsorption or chemical bonding, and then decomposing during the Py-GC/MS experiments which releases the sulfur dioxide gas. A sulfur oxidation mechanism also occurs in the market fuels since sulfur dioxide evolves for all of the deposits in the 400-1050 °C temperature regime. However, the higher concentration of different sulfur molecules in the profouled fuels could lead different deposition mechanisms for the oxidized sulfur compounds which appear to be less stable.

Homologous series of alkyl phenols and alkyl aniline compounds evolve from all of the deposits in the 300-400 °C and 400-1050 °C temperature regimes. It is possible that these polar compounds adsorb strongly to the deposit and only start to desorb at 300-400 °C. However, their presence in the 400-1050 °C temperature regime suggests that they are incorporated into the deposit structure and are being evolved as a result of pyrolytic cleavage. These compounds have been implicated in deposit formation for jet fuel and diesel fuel as well, so it is not surprising that they also could affect deposit formation in gasoline [29,30].

Deposited-Injector Impacts on Spray Morphology

To support the evaluation of impacts of injector deposits on injector performance, and in particular the fuel-injection and mixture-preparation process, the free-spray behavior of three types of injectors used in this study was measured under engine-relevant conditions. The three injector types chosen for this portion of the study featured different characteristic levels of injector deposits, both from a volumetric standpoint, and as indicated by measured fuel-flow restriction.

1. 2017 Hyundai Tucson – Tested for 8,000-miles with a profouled fuel. Average injector restriction was measured at 10.7%.
2. 2015 BMW B48 – Tested for 96-hours with an additized market fuel. Average injector restriction was measured at 1.1%
3. 2019 Ford Escape – Tested for 200,000-miles with an additized market fuel . Average injector restriction was measured at 12.9%.

The objective of the following work is an analysis of the effect of injector fouling on spray dispersion and liquid penetration. For example, changes in spray delivery created by fouling could create problematic liquid impingement upon in-cylinder surfaces, causing soot formation that is problematic as an emission source but also as a mechanism to produce even more fouling [31]. We explored the selected GDI systems at different in-cylinder conditions to understand how phenomena such as flash-boiling injection may manifest different results for fouled or clean injectors. All of the results are the product of the previously discussed PLV measurements, however, they will be presented with various forms of post-processing including raw images, simple filtering, tomographic reconstruction, and 3D rendering depending on the objective.

Instantaneous raw transmittance measurement data is shown in Figure 15 at various conditions for an injector mounted in the head (the BMW B48) and an injector mounted in the side (Hyundai Tucson) of the engine. With different orientation, the designed hole layout and spray pattern are significantly different for these styles of injectors. For the injector rotations depicted there are overlapping plumes along a line of sight. Nevertheless, pockets of liquid shed and evaporation from single plumes in the turbulent process are evident. The penetration of leading plumes is also apparent, with different plumes leading the way depending upon conditions. For reference, a red line indicates 30 mm and a green line indicates 60 mm downstream of the injector tip. These instantaneous transmittance measurements at a particular time after start of injection (ASOI) are converted to PLV using Equation 1 and Equation 2, and then ensemble averaged from multiple injections.

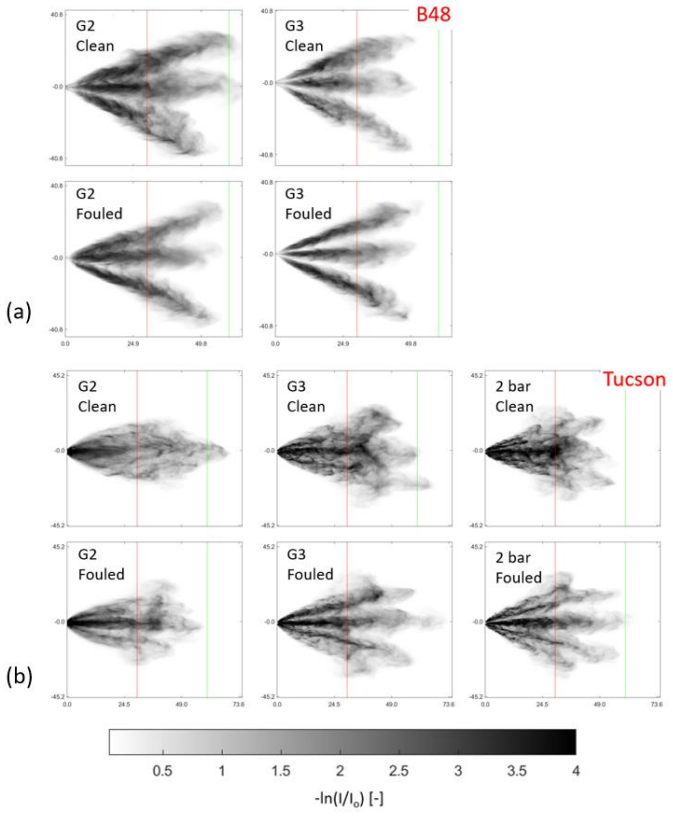

Figure 15. Raw projected intensity ratio for (a) B48, and (b) Tucson injectors under the indicated conditions

The ensemble-averaged PLV images for fouled and clean injectors at various conditions are shown in Figure 16. Evidence of consistent head vortex rollup persists in the ensemble average, but turbulent structure information present in instantaneous images is lost in the averaging. The averaged images provide a quantitative basis for comparison between fouled and clean injector performance. These data are also used at each rotated viewing angle to calculate the 3D computed tomography results.

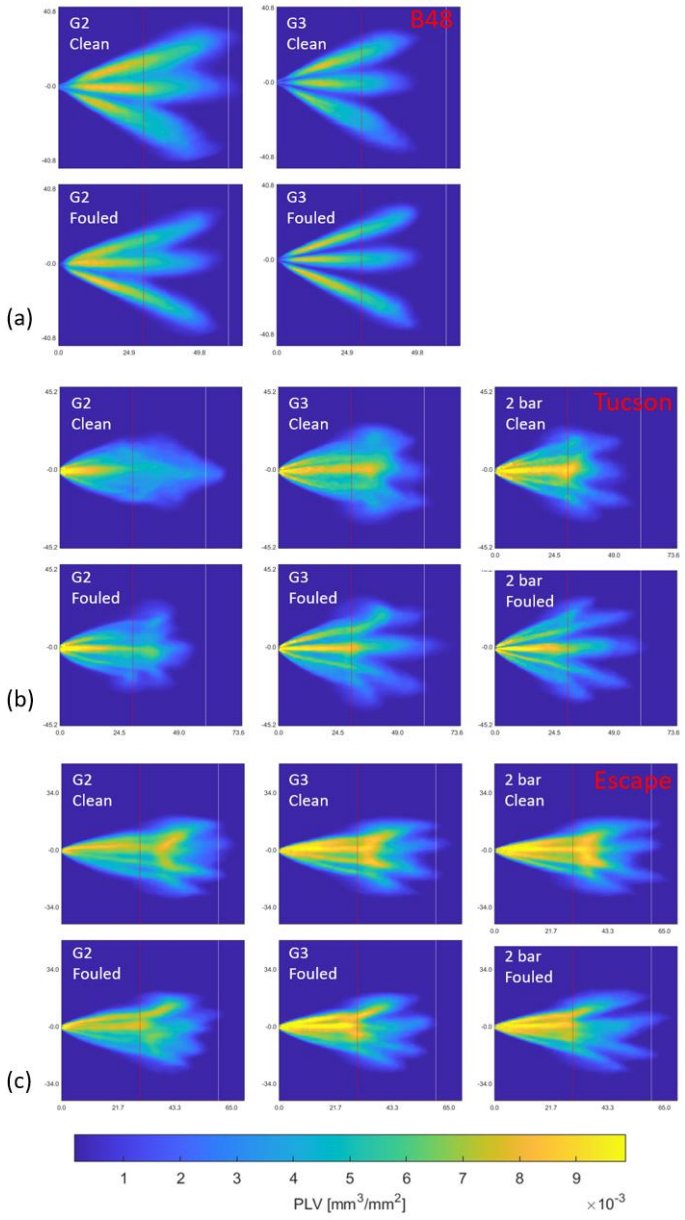

Figure 16. Ensemble-averaged projected liquid volume for (a) B48, (b) Tucson, and (c) Escape injectors under the indicated conditions

Figure 16 shows ensemble-averaged PLV for clean and fouled B48, Tucson, and Escape injectors under G3, G2, and 2 bar conditions. The sample times after start of injection are based on liquid passing out of the viewing window, which depends upon conditions or the end of injection. For reference, a red line indicates 30 mm and a white line indicates 60 mm downstream of the injector tip. Injectors tips are located at (0,0) and firing rightwards. The Tucson injectors are rotated such that the spray is symmetric about the central axis, meaning that plumes normally aimed towards the piston are aimed towards the viewer. The B48 injector is roughly symmetric and is oriented such that the middle plumes are firing towards the viewer. These orientations were chosen to maximize clarity to distinguish plumes or plume pairs along the line of sight. Even so, in the Tucson case, plumes 2 and 3, 5 and 6, and 1 and 4 are mostly indistinguishable while in the B48 case plumes 1 and 2, 3 and 4, and 5 and 6 are indistinguishable.

For clarity, focus will be on the Tucson and B48 injectors under G3 conditions. The Tucson and B48 injector spray trajectories are significantly different, and the PLV images at one instant in time indicate different dynamics for the plumes. A comparison between the clean and fouled injectors also immediately reveals discernible effects of fouling on the spray. The visible effect of fouling at the bottom in Figure 16 is that the delineation in regions of high liquid volume fraction for the fouled injectors is much more obvious than in the clean injectors. Chasms of low liquid volume fraction between plume centers are much deeper in the fouled images. These regions of liquid fraction dearth appear at the head of the plumes as well as near the injector tip. Consequently, since the injected mass of the fouled and clean injectors is roughly the same, the liquid volume fraction is much more concentrated in the fouled injectors.

Visualization of individual plume behavior is difficult when limited to line-of-sight data, therefore, the 3D post-processing methodology is utilized to provide more detailed evidence of plume dynamics.

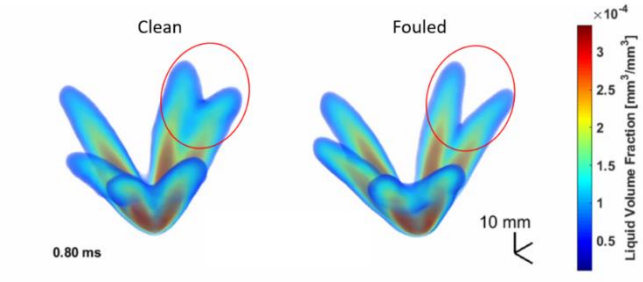

Figure 17. 3D tomographic reconstruction of B48 injector at 0.8ms ASOI under G2 conditions

Figure 17 shows 3D tomographic reconstructed data formatted into a pseudo-3D rendering for the B48 injector. Plumes are semitransparent and colored by liquid volume fraction. The data was sampled at 0.8 ms ASOI for the B48 injector firing upwards under G2 conditions. Identical red rings are placed on the figures to highlight the separation of the plumes in the fouled case compared to the clean case. Although the range of the highlighted plumes of the clean injector has approximately the same maximum extents in the azimuthal direction, in-between the plumes the clean case shows the plumes are much fuller, indicating larger plume cone angle for the clean injector.

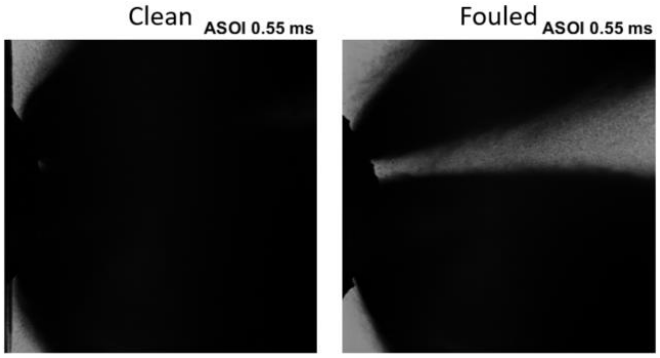

Figure 18. Backlit long-distance microscopy for the BMW B48 injector at G2 conditions. Image width is 3.89 mm.

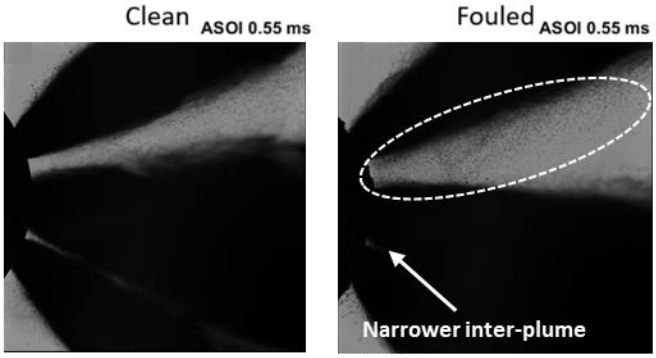

Figure 19. Backlit long-distance microscopy for the BMW B48 injector at G3 conditions. Image width is 3.89 mm.

Figure 18 shows unprocessed images of the clean and fouled B48 injector produced using long range microscopy at 0.55 ms ASOI under G2 conditions. Both injectors are clocked at the same angle,

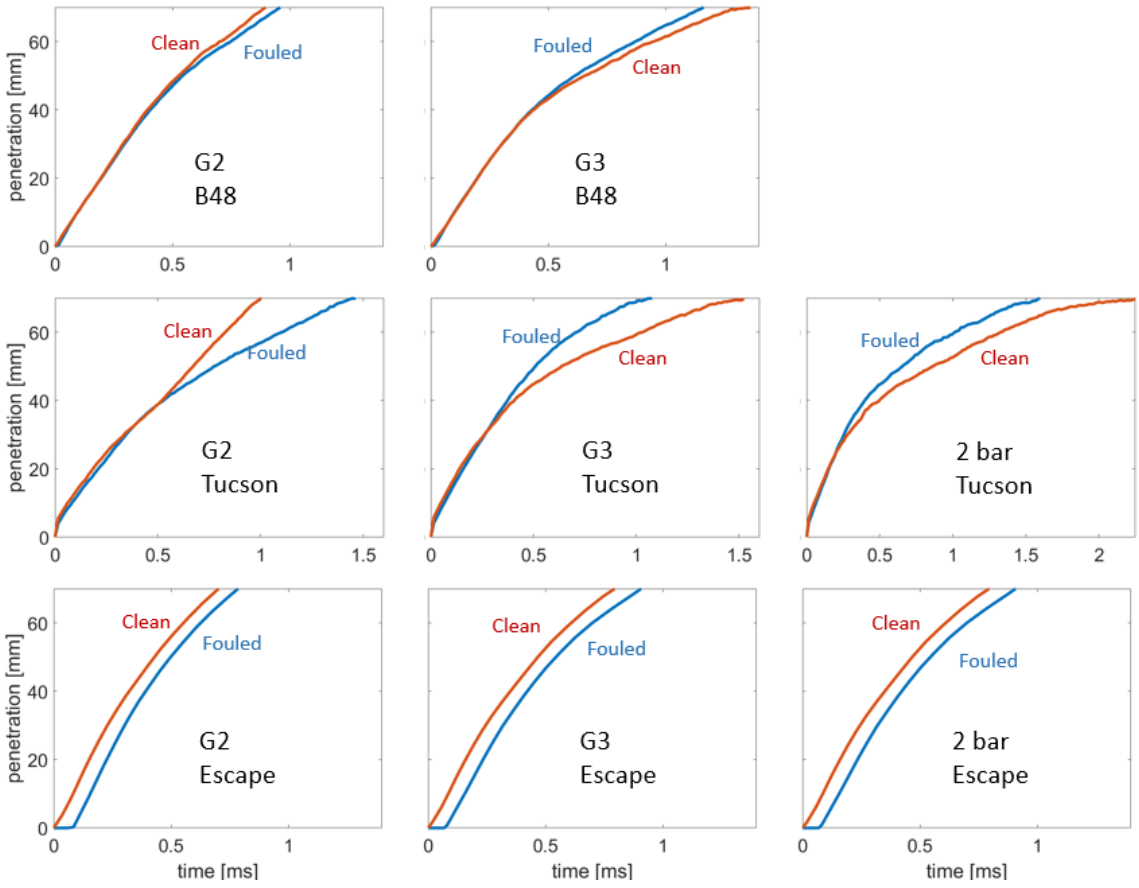

Figure 20. PLV penetration plots with a threshold of 2e-4mm3/mm2 and from the perspectives and conditions shown in Figure 1. (top) B48, (middle) Tucson, and (bottom) Escape injectors

such that two plumes are firing upwards and four are firing downwards, with two plumes projecting on each other along the line of sight. Despite having the same vantage point, a gap between the two upward and four downward firing plumes is only visible in the

fouled injector. In addition, the overall width of the clean injector is also larger than the fouled injector. Consistent with Figure 16 downstream, it is clear that individual plumes for the fouled injector are not as wide as that of the clean injector, even immediately after the counter bore exit of the hole. The thinner plumes from fouled injector restricted plume-to-plume interaction and prevented complete plume collapse. Thus, the liquid penetration length was shorter with the fouled injector under flash-boiling condition. In terms of air-fuel mixing, however, it is noted that fouled injector causes deterioration in atomization showing larger droplets and liquid ligaments. In the previous research of Zhou et al. [32], the fouled injector showed split flow and larger droplets compared to the clean injector. A similar trend was captured in this study. The fouled injector had larger droplets detached from main plumes that filled the inter-plume space as shown in Figure 19.

Figure 20 compares the spray penetration length over time for fouled and clean injectors under 2 bar, G3, and G2 conditions for all injectors. The spray penetration length is determined by the furthest downstream location with a PLV below a threshold of 2e-4 mm^3/mm^2 using the same projection direction used in Figures 15 and 16. This definition is consistent with ECN standards to define maximum liquid penetration length [25], but at the G2 and G3 conditions liquid vaporization is incomplete and the lower value really marks the extent of liquid or vapor penetration within 70 mm distances during injection [23]. The penetration lengths seen in G3 surfaces of Figure 16 can be corroborated with the plots of Figure 20. B48 and Tucson injectors share a behavior that will be discussed in length. However, the Escape injector has a different, prominent feature. As such, the Escape injector will be examined first and then the other injectors will be focused on in the remainder of the paper.

The most discernible difference between the Escape clean and fouled injector penetration profiles is a distinct delay in injector opening and penetration for the fouled injector. In the plots of Figure 20, time is defined as the time after start of injection for the clean injector (not the fouled injector), indicating that the fouled injector has a delayed opening by approximately 75 µs. After this delay to opening, the penetration is quite rapid, reaching beyond 70 mm in less than 1 ms. However, the shape of the penetration is quite similar for either clean or fouled injectors. We therefore look primarily for reasons why injector fouling and aging may cause a change in the hydraulic opening of the injector, as it does not look like there is measurable change in relative penetration speed after injector opening.

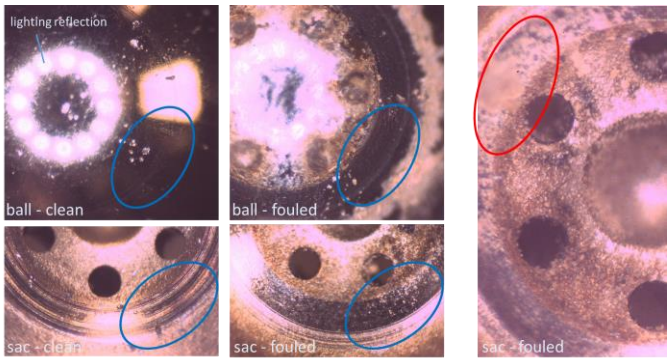

Figure 21. Microscopy images of disassembled Ford Escape injector ball and sac with wear pattern highlighted in blue. Fouled injector shows deeper wear pattern and a lacquer-like deposits and fouling including the seat region highlighted in red

A possible explanation for the altered hydraulic delay for the Escape fouled injector comes from examination of the ball and sac seating surface internal to the injector. Figure 21 shows microscopic imagery of the fouled and clean injector ball and sacs. This internal injector imaging was possible only through destructive disassembly, post-testing. Highlighted in the images are the seating surfaces of the ball. In the clean injector, a single line of contact is barely visible. In the fouled injector the line has become a wide band with a noticeable change in normal distance to injector holes. The wear marks for seating on the ball are clearly at a higher radial distance for the clean injector compared to the fouled injector. For the fouled injector, the wear lines in the sac are also closer to the holes and there are actually corresponding impressions for each of the holes evident in deposits on the ball. Note that these are distinguishable from lighting reflections (from a ring light) indicated on the images. Finally, other imaging of the sac at higher magnification shows evidence of thick deposits and wear deep in the sac region.

The overall wear pattern suggests a “dragging” of the seating area including a deeper stroke of the sealing ball/needle. This longer stroke would necessarily change the injection profile, albeit to a questionable degree. The moving ball would need to clear the deeper seat into the sac as well as the built-up deposit before fuel would flow freely and completely into the sac and holes. Depending on the surface roughness, an increase in static friction is suspected. These dynamics can contribute to an overall “stiction” that delays opening of the fouled injector.

Returning to Figure 20, with the focus now on the B48 and Tucson injectors. All figures show approximately identical injection profiles for clean and fouled injectors until approximately 0.4 ms ASOI. Then there is a notable shift-change in injection profiles and deviation becomes more apparent. The B48 injector shows less penetration length sensitivity to its fouling compared to the Tucson injector. For either injector, penetration eventually leads for the fouled injector at G3 conditions. G2 conditions for the Tucson injector shows the same. A logical explanation for this behavior is that narrow plumes from the fouled injector penetrate faster than larger plumes (i.e. larger plume cone angle) from the clean injector. However, the trend reverses for the G2 conditions, with a faster penetration for the clean injector. Understanding this dynamic requires not only understanding of individual plume behavior, but of the tendency for plumes to merge together with different spray patterns and plume spacings, as discussed next.

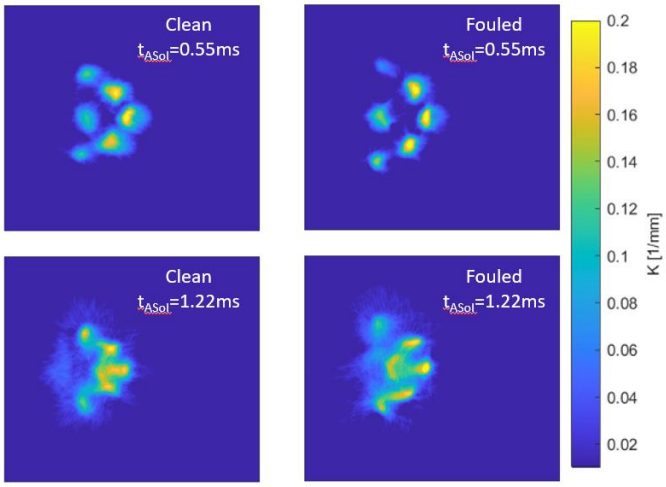

Figure 22. Surfaces colored by the extinction coefficient at the axial cross-sectional plane 30mm downstream under G3 conditions. 0.55ms ASoI (top), 1.22ms ASoI (bottom), Clean case (left), Fouled case (right)

We depict the interaction between plumes by showing measured LVF at select axial planes and timings. Figure 22 features the Tucson injector at G3 conditions. Recall that penetration is ultimately highest for the fouled injector at this condition. Figure 20 shows an axial plane 30 mm downstream, with surfaces colored by LVF at timings of 0.55 and 1.22 ms ASOI for the clean and fouled injectors. Videos of the same plane but spanning 0 to 2 ms ASOI are available at [25]. At 0.55 ms ASOI, all of the six plumes are easily identifiable and separated for the clean and fouled cases. The plume width of the clean injector is wider. The trajectories of the fouled injector plumes are slightly more dispersed, but also less consistent. At 1.22 ms ASOI (near the end of the plotted penetration in Figure 20) both the fouled and clean cases show a migration of plumes towards a central point, but not a complete merging between plumes. The clean case is more symmetric and compact, meanwhile, Plumes 2 and 6 in the fouled case are noticeably more independent than in the clean case.

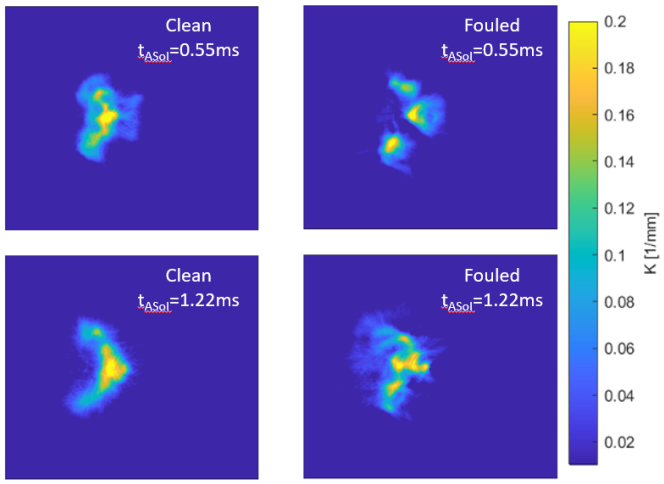

Figure 23 Surfaces colored by LVF of the axial cross-sectional plane 30mm downstream under G2 conditions. 0.55ms ASoI (top), 1.22ms ASoI (bottom), Clean case (left), Fouled case (right)

Figure 23 shows surfaces colored by LVF of the axial plane 30 mm downstream and at 0.55 and 1.22 ms ASOI of the fouled and clean Tucson injectors under G2 conditions. Videos of the same plane but spanning 0 to 2 ms ASOI are also available [25]. At 0.55 ms ASOI there has already been a significant migration of plume centers. The clean case shows all plumes forming a cohesive entity while the fouled case shows a distinct separation between three entities where the top and bottom entities are composed of plumes 2 and 6. This is in stark contrast to the parallel figures under G3 conditions where plumes were much more independent. At 1.22 ms ASOI the plume migration is approaching an asymptote and the boundaries have become more defined. The clean case is much more homogeneous with shallower internal gradients while the fouled case has substantial stratification throughout.

Spray Morphology Analysis

Clean injectors have a larger plume angle as shown in Figures 15, 16, 17, 22, and 23. When the plumes are close enough, the wider, clean-case plumes drive more interaction between plumes. Touching plumes are drawn towards each other and may eventually collapse [23]. The flash boiling G2 conditions results in larger plume angle growth [23] and greater interaction between plumes can be expected, as was demonstrated in Figure 18. For the Tucson injector, where the plumes are in closer proximity to each other compared to the B48 injector, there is an immediate and more complete plume interaction at G2 conditions compared to G3 conditions (compare Figure 22 versus Figure 23), particularly for the clean injector where each plume has a larger baseline cone spreading angle. Once the plumes have collapsed, a common average velocity profile across all the advecting fluid with less velocity stratification is formed. More fluid moves in shallower velocity gradients resulting in less efficient momentum exchange with the ambient gas along the periphery. Effectively, at the G2-clean conditions, the collapsed plumes penetrate together with the collective momentum of multiple plumes rather than that of isolated plumes. This results in more momentum driving forward, and faster penetration for this particular G2 condition.

Without full plume collapse at the G3 and 2 bar conditions, the clean-injector plumes are still wider but contribute little to a collective momentum. This results in a more efficient momentum exchange with the ambient gas for each plume, and slower penetration relative to the more compact fouled plumes. Migrating plumes have an additional handicap over constant trajectory plumes in that migrating plumes exchange momentum with previously stagnant ambient gas along their migrating perimeter. Under G3 conditions, clean-injector plume collapse is not immediate and not much more substantial than the fouled case as seen in figure 23. This results in slower penetration for the clean cases as seen in Figure 20.

The same basic arguments apply to the B48 injector, but the ultimate effect on penetration is smaller because of differences in the plume layout. The B48 injector has much less opportunity for collapse than the Tucson injector because of larger designed separation between plumes. In particular, Figure 16 shows significant plume interaction between only two plumes for the B48 injector, rather than four or more plumes for the Tucson injector at the same conditions. Fewer interacting and collapsing plumes means less collective momentum can be leveraged. While fouling modifies the plume growth rate for all injectors, as well as the plume direction, the effect on penetration is less sensitive because of overall plume layout design for the B48 injector.

Summary and Conclusions

Is there a detectable and significant difference in the deposits formed through the use of a profouled fuel, containing an artificially higher amount of sulfur than would be expected in market fuels? Using both market- and profouled fuels for experimental investigations, we approached this question in the following ways:

1. Assessing the injector restriction and comparing flow restriction to the injector tip deposit volume.

2. Chemical analysis of the deposits that are formed on the tip of the injector.

3. Spray morphology analysis of the injectors, restricted using the different fueling methods.

Analysis of the injector-tip deposits indicated that profouled fuel, made through the use of a sulfur dopant, may create a higher deposit volume on the injector tip than market fuels. This is seen by comparison of injectors run with profouled fuel over short test durations compared with injectors run with market fuels over short and long test durations. Additionally, Py-GC/MS chemical analysis has shown that there is a chemical difference in the formed tip deposits, namely that SO_2 begins evolving from the injector tip deposits at a lower temperature regime when formed using a profouled fuel than when formed with a market fuel.

While differences in both the chemistry of the deposits and their volume are present, are they significant? We evaluated this question by analyzing direct-injector free-spray morphology under engine relevant conditions for injectors from three vehicle types, including both clean injectors as well as injectors fouled with either market fuel or profouled fuel. Each of the analyzed injector types exhibited spray morphology impacts due to the presence of injector deposits, with the most notable impact being a narrowing of the individual spray plumes of fouled injectors, leading to reduced plume-to-plume interaction and altered liquid-spray penetration dynamics, when compared to clean injectors. This held across all tested injectors, regardless of test fuel type, test length, cycle or percent injector restriction.

Injector deposits were observed to impact injector free-spray behavior, both in terms of plume cone angle as well as plume direction. The reduction in spray plume angle and resulting reduction in fuel momentum transfer to the ambient gasses had varying impacts depending on the test conditions. This variation was dependent on whether flash-boiling conditions or high ambient-density conditions were present. Under high-density conditions not exhibiting spray collapse, increased liquid spray penetration was observed. However, under flash-boiling conditions, injector designs with narrow included-spray angle can see a reduction in spray collapse due to reduced plume-to-plume interactions, leading to reduced liquid penetration. These effects were linked to the presence of deposits and can vary by injector design. Further improvement in our understanding of these mechanisms could be addressed in future studies by investigating spray performance impacts due to injector deposit location (e.g. surface vs. counterbore regions).

Additionally, one set of injectors used in this study, which were conditioned with 200,000 miles of vehicle drive-cycle use, were found to exhibit delayed injector opening and start-of-injection response to electrical commands. This behavior likely resulted from mechanical wearing of the internal injector parts, and further altered spray penetration dynamics while also reducing fuel delivery for a given commanded injection pulse-width. However, shot-term testing, carried out with a profouled fuel or a market fuel, will not capture impacts of injector mechanical wear.

The results of this work suggests that while chemical differences between the deposits formed through different fueling strategies exist, both natural and profouled injectors can exhibit significant deposit accumulation and flow restriction. Further, both injectors with and without significant flow restriction can exhibit changes in spray morphology due to injector deposits. In the experiments carried out for this study, no impacts of profouled deposits on injector performance were identified which extend beyond the range of impacts caused by naturally formed deposits. Therefore, the indications from this study are that the use of a profouled fuel for research purposes can be an acceptable option to facilitate research into the formation and impact of injector deposits, when the level of deposit formation and impacts on injectors resembles that which is observed with natural fouling.

References

1. Bruno, B., Santavicca, D., and Zello, J., "Fuel Injection Pressure Effects on the Cold Start Performance of a GDI Engine," SAE Technical Paper 2003-01-3163, 2003, https://doi.org/10.4271/2003-01-3163.
2. Burke, D., Foti, D., Haller, J., and Fedor, W., "Fuel Rail Pressure Rise during Cold Start of a Gasoline Direct Injection Engine," SAE Technical Paper 2012-01-0393, 2012, https://doi.org/10.4271/2012-01-0393.
3. US EPA, "The EPA Automotive Trends Report," The EPA Automotive Trends Report | US EPA, accessed Sept. 2021.
4. Zhao, F., Lai, M.-C., Harrington, D.L., "Automotive spark-ignited direct-injection gasoline engines," *Progress in Energy and Combustion Science*, 25(5):437-562, 1999, https://doi.org/10.1016/S0360-1285(99)00004-0.
5. Whitaker, P., Kapus, P., Ogris, M., and Hollerer, P., "Measures to Reduce Particulate Emissions from Gasoline DI engines," *SAE Int. J. Engines* 4(1):1498-1512, 2011, https://doi.org/10.4271/2011-01-1219.
6. Sobotowski, R., Butler, A., and Guerra, Z., "A Pilot Study of Fuel Impacts on PM Emissions from Light-Duty Gasoline Vehicles," *SAE Int. J. Fuels Lubr.* 8(1):214-233, 2015, https://doi.org/10.4271/2015-01-9071.
7. Coordinating Research Council, "E-94-2: Evaluation and Investigation of Fuel Effects on Gaseous and Particulate Emissions on SIDI In-Use Vehicles," CRC_2017-3-21_03-20955_E94-2FinalReport-Rev1b.pdf (wpengine.com), accessed Sept. 2021.
8. Coordinating Research Council, "E-94-3: Impacts of Splash-Blending on Particulate Emissions for SIDI Engines," SwRI (wpengine.com), accessed Sept. 2021.
9. Coordinating Research Council, "E-129: Alternative Oxygenate Effects on Emissions," CRC-Project-E-129-Final-Report_May-2019.pdf (wpengine.com), accessed Sept. 2021.
10. Berndorfer, A., Breuer, S., Piock, W., and Von Bacho, P., "Diffusion Combustion Phenomena in Gdi Engines caused by Injection Process," SAE Technical Paper 2013-01-0261, 2013, https://doi.org/10.4271/2013-01-0261.

11. Xu, H., Wang, C., Ma, X., Sarangi, A., Weall, A., Krueger-Venus, J., "Fuel injector deposits in direct-injection spark-ignition engines," *Progress in Energy and Combustion Science*, 50: 63-80, 2015 https://doi.org/10.1016/j.pecs.2015.02.002.
12. Henkel, S., Hardalupas, Y., Taylor, A., Conifer, C. et al., "Injector Fouling and Its Impact on Engine Emissions and Spray Characteristics in Gasoline Direct Injection Engines," *SAE Int. J. Fuels Lubr.* 10(2):287-295, 2017, https://doi.org/10.4271/2017-01-0808.
13. Nagano, S., Yokoo, N., Kitano, K., and Nakata, K., "Effects of High Boiling Point Fuel Additives on Deposits in a Direct Injection Gasoline Engine," *SAE Int. J. Fuels Lubr.* 10(3):2017, https://doi.org/10.4271/2017-01-2299.
14. Reid, J., Mulqueen, S., Langley, G., Wilmot, E. et al., "The Investigation of the Structure and Origins of Gasoline Direct Injection (GDI) Deposits.," SAE Technical Paper 2019-01-2356, 2019, https://doi.org/10.4271/2019-01-2356
15. Shanahan, C., Smith, S., and Sears, B., "A General Method for Fouling Injectors in Gasoline Direct Injection Vehicles and the Effects of Deposits on Vehicle Performance," *SAE Int. J. Fuels Lubr.* 10(3):2017, https://doi.org/10.4271/2017-01-2298.
16. Altin O, Eser S. Carbon deposit formation from thermal stressing of petrolelum fuels. Prep. Pap-Am Chem Soc, Div. Fuel Chem 2004;49:765.
17. Fernandes H, Braga LC, Martins AR, Braga SL, Braga CVM. Fuel sulfate content influence in the formation of inorganics components deposits in the engine injectors with technologies of gasoline direct injection. 2013. SAE Technical Paper, No. 2012-36-0314.
18. Carlisle HW, Frew RW, Mills JR, Aradi AA, Avery NL. The effect of fuecomposition and additive content on injector deposits and performance ofan air-assisted direct injection spark ignition (DISI) research engine. 2001.SAE Technical Paper, No. 2001-01-2030
19. Von Bacho, P., Galante-Fox, J., and Sant, D., "Development of a Robust Injector Design for Superior Deposit Resistance," SAE Technical Paper 2005-01-3841, 2005, https://doi.org/10.4271/2005-01-3841.
20. Smocha, R., "Sludge and Varnish Evaluation of Polyether Amine Gasoline Fuel Additives at "Complete Fuel System Cleaner" Aftermarket Fuel Additive Concentrations," SAE Technical Paper 2020-01-2100, 2020, http://doi.org/10.4271/2020-01-2100.
21. Hwang J, Lee P, Mun S, Karathanassis IK, Koukouvinis P, Pickett LM, et al. Machine-learning enabled prediction of 3D spray under engine combustion network spray G conditions. Fuel 2021;293:120444. https://doi.org/10.1016/j.fuel.2021.120444.
22. Weiss L, Wensing M, Hwang J, Pickett LM, Skeen SA. Development of limited-view tomography for measurement of Spray G plume direction and liquid volume fraction. Exp Fluids 2020;61:1–17. https://doi.org/10.1007/s00348-020-2885-0
23. Hwang J, Weiss L, Karathanassis IK, Koukouvinis P, Pickett LM, Skeen SA. Spatio-temporal identification of plume dynamics by 3D computed tomography using engine combustion network spray G injector and various fuels. Fuel 2020;280:118359. https://doi.org/10.1016/j.fuel.2020.118359..
24. Pickett LM, Genzale CL, Manin J. Uncertainty quantification for liquid penetration of evaporating sprays at diesel-like conditions. At Sprays 2015;25:425–52. https://doi.org/10.1615/AtomizSpr.2015010618.
25. Engine Combustion Network webpage [https://ecn.sandia.gov/gasoline-spray-combustion/target-condition/spray-g-parametric-variation/]
26. Lopez Pintor, D., Dec, J., and Gentz, G., "Experimental Evaluation of a Custom Gasoline-Like Blend Designed to Simultaneously Improve ϕ-Sensitivity, RON and Octane Sensitivity," *SAE Int. J. Adv. & Curr. Prac. in Mobility* 2(4):2196-2216, 2020, https://doi.org/10.4271/2020-01-1136.
27. Fuchs, W., & Sandhoff, A. G. (1942). Theory of Coal Pyrolysis. Industrial & Engineering Chemistry, 34(5), 567-571. doi:10.1021/ie50389a010
28. "Co-Optimization of Fuels & Engines: FY16 Year in Review," Report No. NREL/BR-5400-67595, National Renewable Energy Laboratory, 2017
29. Christison, K. M., Lorenz, R. M., Xue, L., & Sparkman, O. D. (2019). Exploring the Molecular Origin of Jet Fuel Thermal Oxidative Instability through Statistical Analysis of Mass Spectral Data. Energy & Fuels, 33(2), 830-836. doi:10.1021/acs.energyfuels.8b03670
30. Batts, B. D., & Fathoni, A. Z. (1991). A literature review on fuel stability studies with particular emphasis on diesel oil. Energy Fuels, 5(1), 2-21. doi:10.1021/ef00025a001
31. Kim, N., Vuilleumier, D., and Sjoberg, M., "Effects of Injection Timing and Duration on Fuel-Spray Collapse and Wall-Wetting in a Stratified Charge SI Engine," SAE Technical Paper 2021-01-0544, 2021, https://doi.org/10.4271/2021-01-0544
32. Jianwei Zhou, Yiqiang Pei, Zhijun Peng, Yanfeng Zhang, Jing Qin, Li Wang, Changwen Liu, Xiaoyu Zhang, Characteristics of near-nozzle spray development from a fouled GDI injector, Fuel, Volume 219, 2018, Pages 17-29, ISSN 0016-2361, https://doi.org/10.1016/j.fuel.2018.01.070.

Contact Information

Ruth Smocha
Fuels Engineer
Chevron Corporation
ruthsmocha@chevron.com

Acknowledgments

Thank you to Majid Ahmadi, Doug Cyr, Andrew Ickes, Brian Morlan, Abraham Zepada for supporting the activities related to this study.

Definitions/Abbreviations

DISI	Direct Injection Spark Ignition
PFI	Port Fuel Injection
CCD	Combustion Chamber Deposits
OEM	Original Equipment Manufacturers
PAH	Polyaromatic Hydrocarbons

PM	Particulate Matter
LIF	Laser Induced Fluorescence
PN	Particulate Number
RDE	Real Driving Emissions
DCA	Deposit Control Additive
DTBDS	di-tert-butyl disulfide
TBHP	tert-butyl hydrogen peroxide
FTIR	Fourier Transform Infrared Spectroscopy
MY	Model Year
MAD	Mileage Accumulation Dynamometer
LTFT	Long Term Fuel Trim
Py-GC-MS	Pyrolysis-Gas Chromatography-Mass Spectrometry
GC-DHA	Gas Chromatography Detailed Hydrocarbon Analysis
LED	Light-Emitting Diode
CT	Computed Tomography
PLV	Projected Liquid Volume
LVF	Liquid Volume Fraction
RTICC	Reconstructed Total Ion Current Chromatograms
ASOI	After Start Of Injection

Supplemental Information

S.1 Figures from Py-GC/MS Analysis

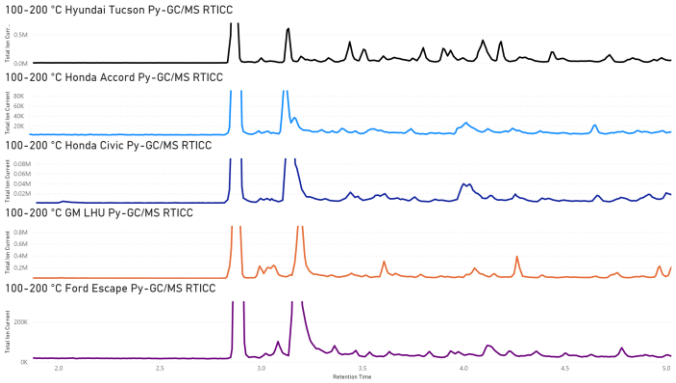

Figure S.1. Comparison of the First Time Region of the RTICCs from all injector tip deposits in the 100-200 °C Py-GC/MS temperature regime. The peak at 2.1 min in the RTICC for the Hyundai Tucson has a mass spectrum consistent with 2-methylbutane. The peaks for the other 4 deposits in this same area have mass spectra consistent with ethanol.

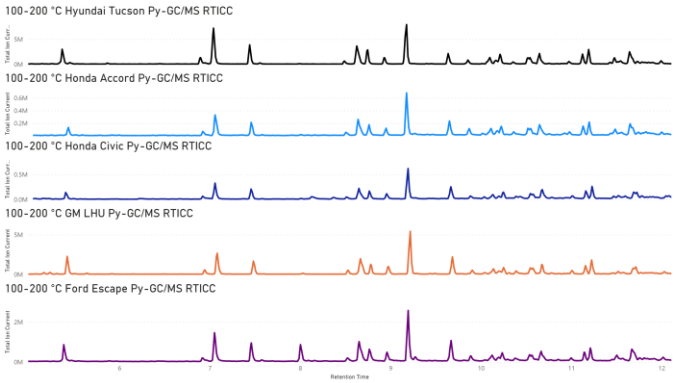

Figure S.2. Comparison of the Second Time Region of the RTICCs from all injector tip deposits in the 100-200 °C Py-GC/MS temperature regime. These peaks all have retention times and mass spectra consistent with mononuclear aromatic compounds

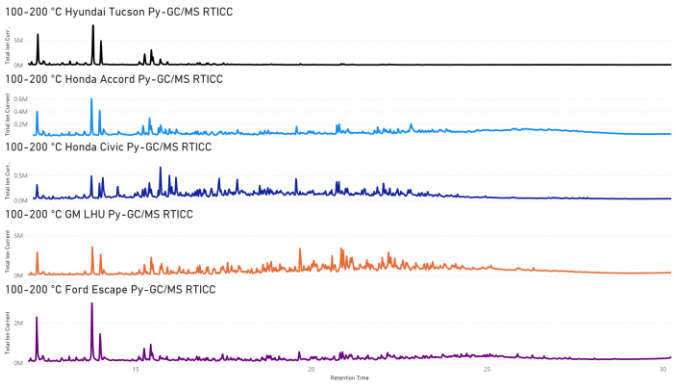

Figure S.3. Comparison of the Third Time Region of the RTICCs from all injector tip deposits in the 100-200 °C Py-GC/MS temperature regime. From 12-15 min have mass spectra consistent with dinuclear aromatic compounds. Peaks after 15 min have mass spectra consistent with polynuclear aromatics.

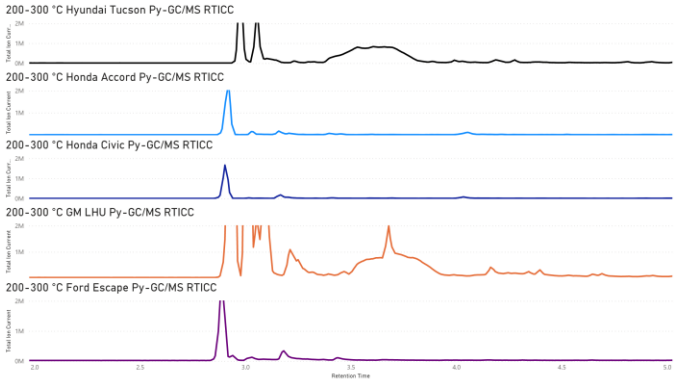

Figure S.4. Comparison of the First Time Region of the RTICCs from all injector tip deposits in the 200-300 °C Py-GC/MS temperature regime. The broad peaks from approximately 3.5-4.0 minutes have mass spectra consistent with SO_2.

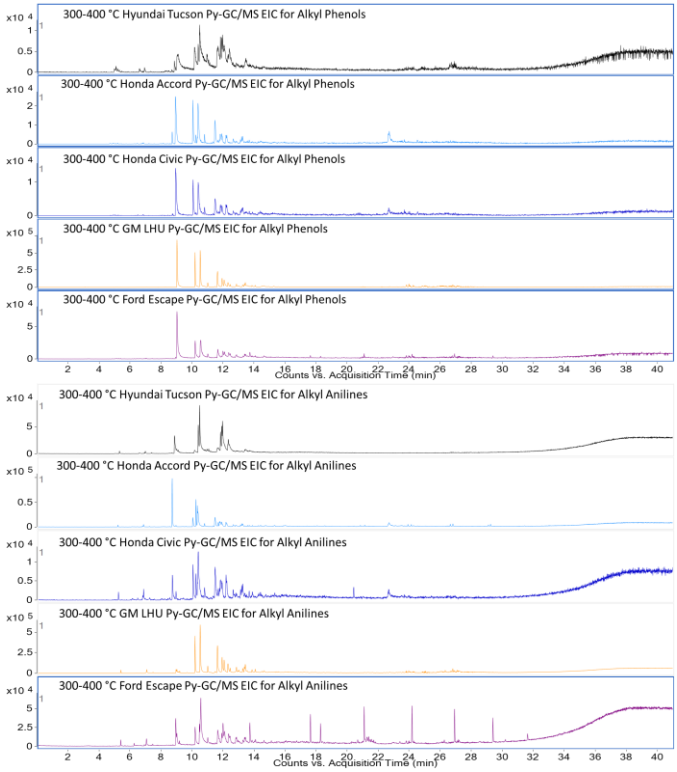

Figure S.5. EICs for alkyl phenols (*m/z* 94, 108, 122, 136) and alkyl anilines (*m/z* 93, 107, 121, 135) 300-400 °C

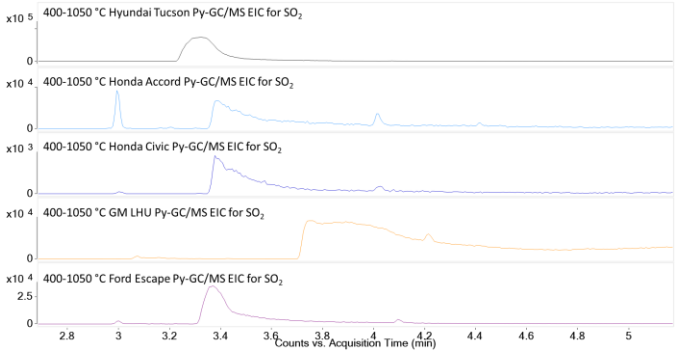

Figure S.6. EICs for SO_2 (*m/z* 64) 400-1050 °C